Optical absorption in monolayer SnO_2

C. E. Ekuma*
U.S. Army Research Laboratory, Aberdeen Proving Ground, Maryland 21005-5069, USA

(Received 20 August 2018; revised manuscript received 4 November 2018; published 14 February 2019)

Since the discovery of graphene, considerable research efforts have focused on understanding the properties of other two-dimensional materials. Herein, based on *ab initio* many-body calculations, we report the optical properties of monolayer SnO_2. First, we apply the first-principles density functional theory, self-consistent quasiparticle Green's function, and screened Coulomb method to determine the quasiparticle electronic structure. Second, we solve the Bethe-Salpeter equation to obtain the absorption spectra. The quasiparticle band structure reveals an indirect quasiparticle band gap. The absorption spectra show that the direct optical excitation is characterized by an optical band gap of ∼5.36 eV, which is dominated by strongly bound excitons.

DOI: 10.1103/PhysRevB.99.075421

Stannic oxide (SnO_2) is an environmentally friendly, earth-abundant polymorph of tin oxide. It is an important semiconducting metal oxide with a bulk band gap of ∼3.6 eV [1]. SnO_2 has been extensively studied both as a candidate material for fundamental research and for practical applications. It is widely used as a major component material in solid-state chemical and gas sensing [2], solar cells [3], transparent conducting oxides and electrodes [4,5], catalysis [6], and antistatic coatings [7]. In the past decades, nanostructures of SnO_2-based materials have also been synthesized and studied (see, e.g., Refs. [8,9]). With the advent of two-dimensional (2D) materials, which offer far more flexibility to tune the optoelectronic properties, an opportunity is on the horizon to further engineer SnO_2-based devices at the ultimate limit of a discrete atomic layer. Herein, using the state-of-the-art first-principles many-body calculations, we report the optical properties of monolayer SnO_2.

To simulate the monolayer SnO_2 considered herein, we initially carried out structural relaxation based on density functional theory (DFT) [10] using the Perdew-Burke-Ernzerhof (PBE) [11] exchange-correlation functional. We constructed the monolayer by cleaving along the [001] direction of the bulk crystal with a vacuum size $c \sim 20$ Å along the out-of-plane direction to avoid the artifacts of the periodic boundary condition. The cutoff energy E_s for the plane-wave basis set is 550 eV and a $15 \times 15 \times 1$ Monkhorst-Pack grid was used to represent the reciprocal space. The orbitals used in the structural relaxation and self-consistent calculations are between parentheses for Sn ($4s^2\,4p^6\,4d^{10}\,5s^2\,5p^2$) and O ($2s^2\,2p^4$). The monolayer structure is relaxed until the energy (charge) is converged to within $\sim 10^{-4}$ (10^{-9}) eV and the forces dropped to $\sim 10^{-3}$ eV/Å. The predicted monolayer crystal exhibits a D_{3d} (space group no. 164) hexagonal structure with a lattice constant of 3.27 Å and Sn-O bond length of 2.14 Å [Fig. 1(a)].

Obtaining full convergence of excitation energies in 2D materials is challenging. It is well known that the quasiparticle band gap converges rather slowly with the size of the vacuum and an unusually fine reciprocal space grid is needed to achieve a satisfactory convergence [12–14]. In order to determine a reasonable set of input parameters that balance accuracy and the huge computational demand of our many-body calculations, we carried out a series of benchmarking calculations by carefully checking the convergence of the spectra on various computational parameters, such as spin-orbit interactions, the energy cutoffs, Brillouin zone (BZ) sampling grid, additional empty states for the Green's function and screened Coulomb interactions calculations, and the solution of the Bethe-Salpeter equation. We checked the effects of spin-orbit coupling (SOC) at the DFT level using PBE functional. While the SOC induced a slight downward shift in the electronic energies including the splitting of the degenerate state at the valence band extremum of the **K** point in the high symmetry zone, the energy band gap remained practically unchanged $\Delta E_g^{\mathrm{PBE}} \sim 2.48$ meV [Fig. 1(b)]. Hence, we have not included SOC in our subsequent calculations since the effects are negligible. Also, this will reduce the computational cost by at least a factor of 2 since the self-consistent quasiparticle Green's function plus screened Coulomb interactions and vertex corrections scales as $\sim N^6$, where N is the number of bands included in the calculations. We next carried a series of self-consistent calculations presented in Fig. 2 for the convergence of the fundamental quasiparticle band gap at the "one-shot" Green's function and screened Coulomb interactions (G_0W_0) level of approximation as a function of (a) energy cutoff using a grid and vacuum size of 144 k points and 20 Å, respectively, (b) vacuum size with E_s and grid size of 550 eV and 144 k points, respectively, and (c) Brillouin zone sampling grid with E_s and vacuum size of 550 eV and 20 Å, respectively. As expected, the quasiparticle band gap is observed to converge slowly with respect to the aforementioned input parameters. Our calculations also verified that at least 108 bands and 12 virtual and occupied bands, respectively are converged enough for the many-body calculations. A compromised input parameter of $E_s \sim 550$ eV, $c \sim 20$ Å, and BZ sampling of 225 k points are found to be converged and have been used for the results presented herein.

*cekuma1@gmail.com

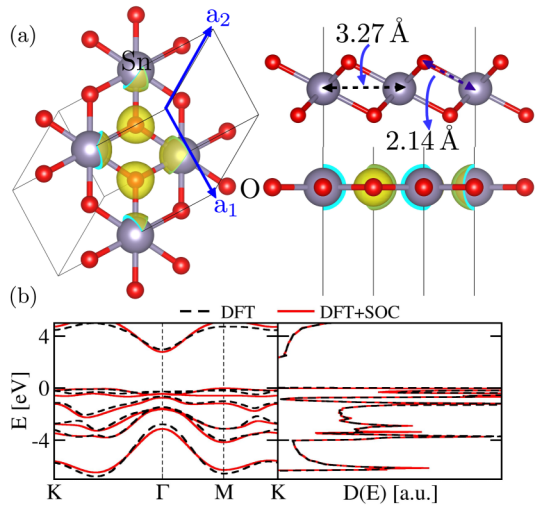

FIG. 1. (a) Top, side, and perspective views of the D_{3d} hexagonal crystal structure of monolayer SnO_2. The blue colored arrows highlight the unit cell defined by the lattice vectors $\vec{a}_1$ and $\vec{a}_2$. (b) A comparison plot of the electronic properties of monolayer SnO_2 obtained using the density functional theory (DFT) with (solid red line) and without (black dashed line) the effects of spin-orbit coupling (SOC).

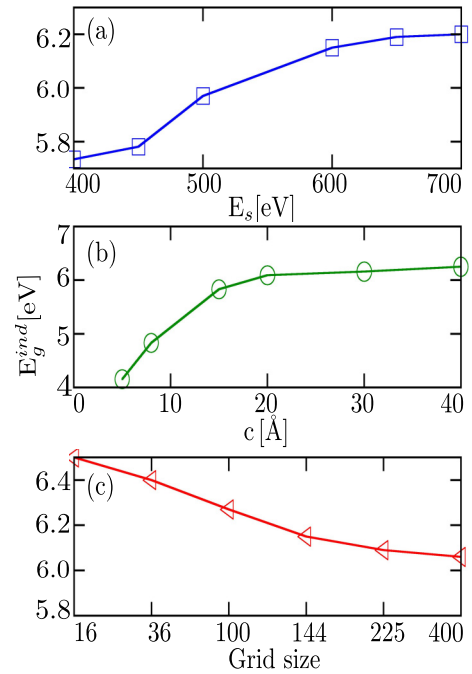

FIG. 2. Convergence of the fundamental energy band gap E_g^{ind} calculated at the G_0W_0 level as a function of (a) energy cutoff E_s with grid and vacuum size fixed at 144 k points and 20 Å, respectively, (b) out-of-plane lattice constant (size of vacuum) with E_s and grid size fixed at 550 eV and 144 k points, respectively, and (c) grid size (Brillouin zone sampling grid) with E_s and vacuum size fixed at 550 eV and 20 Å, respectively. A compromised input parameter of $E_s \sim 550$ eV, $c \sim 20$ Å, and BZ sampling of 225 k points are converged enough and have been used for the results presented herein.

The self-consistency calculations are carried out by combining DFT and self-consistent quasiparticle Green's function plus screened Coulomb interactions (sqGW), which also accounted for vertex correction [15] using an energy cutoff of $2/3E_s \sim 367$ eV and 144 bands to compute the quasiparticle electronic structure. The vertex correction accounts for the polarization (electron-hole interaction) effects beyond the leading order of the perturbation theory (see, e.g., Refs. [16–19]). The sqGW approach obtains the GW eigenstates by a self-consistently determined Hermitian one-electron Hamiltonian approximation to the self-energy [20]. In our case, the one-electron energies and one-electron orbitals are updated four times. Subsequently, we solved the Bethe-Salpeter equation (BSE) [21] using 20 virtual and occupied bands, respectively to obtain the absorption spectra. Aside from the structural optimization, all calculations include an accurate account of electron-electron and electron-hole interactions, and an optimized set of potentials to properly account for excited-state properties. The above calculations were done using the VASP electronic structure suite [22]. The input files for the calculations are provided in the Supplemental Material [23].

An important quantity in characterizing a 2D material is the exfoliation energy, which is the ability of such atomic layer crystal to be obtained from the bulk. The exfoliation energy is the energy required to peel off an atomic layer from the surface of a bulk material. The exfoliation energy is crucial for the optimization process of producing 2D crystals as it provides an experimental guide to the ease of removing an atomic layer from the surface of the corresponding bulk material. Several approaches have been proposed to calculate the exfoliation energy [24–26]. Herein, we calculate the exfoliation energy as the difference in the ground-state energy per unit atom between bulk SnO_2 and the corresponding monolayer similar to the one used in Ref. [24]. We obtain the exfoliation energy per unit area as $\Delta E_{\text{exf}} = [E_m - E_{bm}]/\mathcal{A}$, where E_m (E_{bm}) is the monolayer (bulk) ground-state energy per unit atom and $\mathcal{A}$ is the surface area of the monolayer unit cell. Our calculation led to a $\Delta E_{\text{exf}} \approx 0.29\,\text{Jm}^{-2}$, which is smaller than the ΔE_{exf} in the range 0.34–0.46 Jm^{-2} and $\Delta E_{\text{exf}} \sim 0.45\,\text{Jm}^{-2}$ reported for graphene and hexagonal boron nitride, respectively [24,25] but slightly higher than $\sim 0.17\,\text{Jm}^{-2}$ reported for monolayer MoS_2 [24]. Such ΔE_{exf} implies that a small energy cost is needed to cleave an atomic layer from the surface of bulk SnO_2. In order to ascertain the bonding character of monolayer SnO_2, we carried out charge transfer calculations using the net atomic charge approach [27]. Our calculations suggest a net charge transfer of 1.66 $|e|$ from Sn to an O atom with a bond order sum of 3.51 (1.80) for Sn (O), which implies mixed covalent-ionic bonding in monolayer SnO_2.

Next, we investigate the electronic properties. Both in experimental and computational studies, the electronic properties seem to be the most essential as it serves as the input in diverse material characterizations. For example, the electronic band gap is vital in the accurate characterization of the absorption spectra including the determination of the optical band gap. In order to ensure an accurate determination of the electronic properties, we have instead adopted a version of the GW approach which uses the quasiparticle eigenstates to

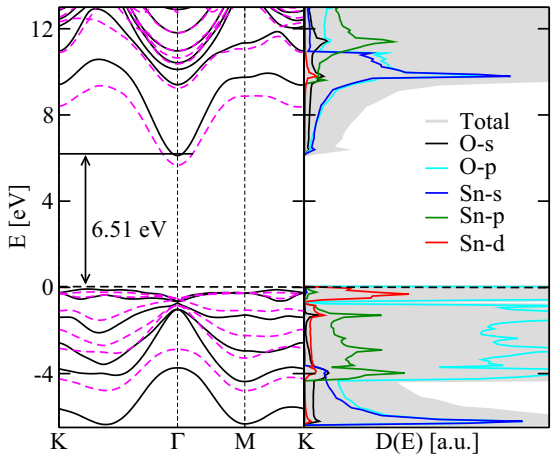

FIG. 3. The electronic properties of monolayer SnO_2 showing the quasiparticle band structure (left panel) and the total and partial density of states (right panel). The spectra exhibit an indirect quasiparticle bandgap $E_q^{\text{ind}} \approx 6.51$ eV along the Γ-K of the k space. The horizontal dashed black line is the Fermi level E_F, which has been set to the top of the valence band.

self-consistently calculate the quasiparticle properties including accounting for vertex corrections [15].

We show in Fig. 3 the electronic properties of monolayer SnO_2 obtained from our many-body calculations. The left panel depicts the quasiparticle band structure. The dashed magenta line is the corresponding band structure obtained from G_0W_0 calculations. Our many-body sqGW calculations predict an indirect quasiparticle band gap of 6.51 eV along the $\Gamma - K$ of the k space, which is higher than the 2.38, 3.89, and 6.19 eV obtained from our PBE, HSE06 hybrid functional [28], and G_0W_0 calculations, respectively. The direct quasiparticle band gaps are 6.92, 6.50, 4.41, and 2.91 eV for sqGW, G_0W_0, HSE06, and PBE calculations, respectively. The PBE band gap is consistent with previous ones from semilocal functionals [29,30]. The sqGW direct (indirect) quasiparticle band gap is larger than the G_0W_0 counterpart by 420 (340 meV). Using a 32/33% of the Hartree-Fock mixing parameter as suggested by Ref. [31] for the hybrid calculations, we obtain an indirect (direct) band gap of 4.34/4.42 (4.87/4.95 eV), in agreement with the data of Xiao *et al* [29]. It is well known that the band gap systematically increases as the mixing parameter is increased [32] due to the increase in the Hartree-Fock exchange contribution to the exchange-correlation energy. We observe that the 6.19 eV quasiparticle band gap obtained from our G_0W_0 calculation is ~0.26 eV larger than the results of Xiao *et al.* [29]. There are several potential sources for such difference not limited to the energy cutoff, potential, basis set, Brillouin zone sampling, and most important, the choice of prior self-consistent data used as the starting point in the G_0W_0 calculation. For example, the data of Xiao *et al.* [29] seem not to have accounted for the Sn-d states in their basis set. As explained below, there are strong antibonding Sn-d-O-p interactions especially around the valence band maximum (VBM).

We also checked for the effects of the choice of the starting eigenstates on our GW calculations. Using the results of the default Hartree-Fock mixing parameter of 25% as the starting input, we obtained indirect quasiparticle band gaps of 5.50 and 6.49 eV for the G_0W_0 and quasiparticle self-consistent GW calculations, respectively. While the quasiparticle fundamental band gap obtained using the HSE06 results as the starting input for the G_0W_0 calculation is smaller than that obtained using the PBE as the starting input by ~0.70 eV, that from the sqGW calculation is smaller only by ~0.02 eV. This should not be surprising since the G_0W_0 approximation is strictly a "one-shot" iteration of the self-energy. In practice, it is perturbative and based on a prior self-consistent calculation. As such, the final G_0W_0 result generally depends on the choice of the self-consistent mean field used as a starting point [33]. The dependence of the GW results on the quality of the starting eigenstates makes it all important that some level of self-consistency on both G and W is needed [34] and may even be more crucial in 2D materials due to weaker and nonlocal dielectric screening. The sqGW approach provides a computationally cheaper yet accurate alternative to the fully self-consistent GW calculations. We believe that our predicted quasiparticle properties using the sqGW approximation provide a more complete description of the electronic structure and excitations in monolayer SnO_2.

In the right panel of Fig. 3, we present the partial density of states. The valence band is formed mainly by O-p states. However, around the VBM, there is some density of Sn-d states due to antibonding of Sn-d-O-p interactions [35]. There are also a substantial density of Sn-p and Sn-s states around 1.0 to ~6.0 eV in the valence band. We observed significant O-s states around 5.0 eV, which strongly hybridized with Sn-d states and some density of O-p and Sn-p states around ~16.0–23.0 eV (not shown). In the conduction band, the dominant states are derived from a strong hybridization between O-p and Sn-s states with both being tangible at the conduction band minimum (CBM). States up to 10 eV is derived from the hybridization of the above conduction band states hybridizing with Sn-p and Sn-d states. We further confirmed the decomposition of the density of states using the all-electron WIEN2K electronic structure code [36]. The overall composition of the states forming the band gap is similar to that reported for bulk SnO_2 [1,37,38]. However, a few important differences exist. For example, our calculations show an insignificant contribution from the O-s states around the CBM, which is present in the bulk. We also observed a CBM dominated by a strong hybridization of O-p-Sn-s states. We attribute these differences mainly to the distinct crystal symmetry of bulk and monolayer lattice, where the latter could have stronger crystal field effects [39].

To gain insight into the transport properties of monolayer SnO_2, we calculated the carrier effective mass. The band effective mass m^b is obtained from the quasiparticle band structure (Fig. 3) by fitting a parabola $E_k = \frac{\hbar^2}{2m_0}\vec{k}^T A\,\vec{k}$ to the states around the band extremum (CBM and VBM), where $k = (k_x, k_y)$ is the in-plane k point measured from the band extremum, the eigenvalues of matrix A yield the inverse of the effective masses in the direction of the band curvature, and m_0 is the free electron mass. The obtained m_e^b along k_x (k_y) is 0.57 (0.65) while the corresponding hole effective mass m_h^b is 3.5 (5.2). The large hole effective mass is expected due to the flat band at the VBM. Defining the exciton effective mass

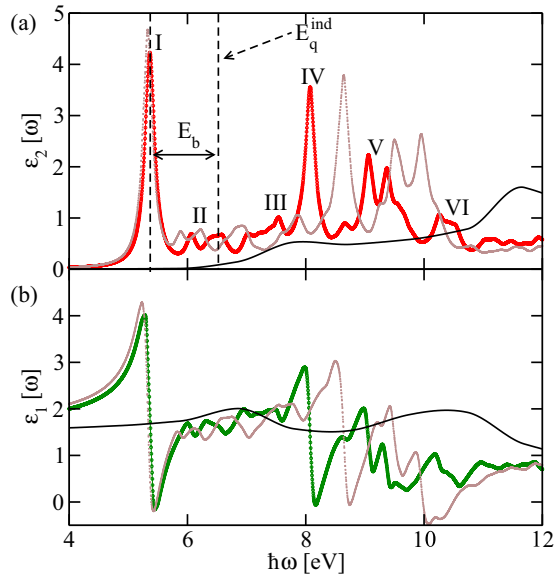

FIG. 4. The optical properties of monolayer SnO_2 showing the (a) imaginary part ε_2 and (b) real part ε_1 of the dynamical dielectric function as a function of the photon energy $\hbar\omega$. The spectra is obtained using DFT+sqGW+BSE calculations. $E_q^{\text{ind}} \sim 6.51$ eV is the quasiparticle band gap obtained from DFT+sqGW and $E_b = 1.15$ is the exciton binding energy. The structure at I in Fig. 4(a) denotes the first direct excitation energy ≈ 5.36 eV. The dashed brown line is the absorption spectra obtained using DFT+G_0W_0+BSE. We also present the absorption spectra without electron-hole interactions obtained using the random-phase approximation (solid black line), which show no structure below the minimal excitation energy (I).

as $\mu^{-1} = m_e^{-1} + m_h^{-1}$, we obtain $\mu \sim 0.49\,(0.58)$ along the k_x (k_y) direction. We note that the electron and hole effective mass obtained using PBE is 0.29/0.57 and 1.08/2.16 along the k_x/k_y, respectively.

The optical spectroscopy, though less direct than the quasiparticle band structure, has the significant advantage of being a true "bulk" probe of the electronic structure of a material. In order to study the absorption spectra of monolayer SnO_2, we calculated the photon-energy dependent dielectric function from DFT, sqGW, and the BSE. The latter is essential to account for the effects of electron-hole interactions, which are important in 2D materials as has been shown by both computations and experiments [40–43]. We are not aware of any reported optical properties of monolayer SnO_2. Given the technological importance of SnO_2, our results provide the needed computational data for the experimental guide in device applications.

The calculated absorption spectra obtained from our DFT+sqGW+BSE calculations are shown in Fig. 4. Also presented in Fig. 4 is the absorption spectra obtained with DFT+G_0W_0+BSE (dashed brown line) and without electron-hole interactions using the random-phase approximation (black solid line) calculations, respectively. The absorption spectra obtained using the BSE theory includes excitonic effects, which lead to a significant increase in the absorbance at the ultraviolet photon energies. On the other hand, the optical spectra obtained using the random-phase approximation (solid black line) show no significant structure in this region of the photon energy. At low energy, the DFT+G_0W_0+BSE spectra are red shifted while at higher energies, they are blue shifted. There are other notable differences especially in the dispersive part of the dynamical dielectric function, including the reversal of peaks to troughs and vice versa at photon energies of 7.98, 8.50, 8.73, and 10.10 eV. The observed deviation from the DFT+G_0W_0+BSE absorption spectra could be due to, among other things, the lack of self-consistency in the "one-shot" GW quasiparticle eigenstates used as input in the calculation of the absorption spectra. We note that these deviations are more pronounced at higher energies. For example, the first excitation energy, even though it is red shifted, only differs from the DFT+sqGW+BSE results by ~70 meV.

The absorptive part of the dynamical dielectric function $\varepsilon_2(\omega)$ [Fig. 4(a)] shows prominent structures labeled I–VI. The lowest sharp structure around 5.36 eV (I) corresponds to the direct optical excitation. Several experimental approaches, e.g., scanning tunneling spectroscopy combined with photoluminescence measurement, could be used to measure the exciton binding energy E_b. The exciton binding energy is a measure of the nature of the electron-hole pair (uncorrelated or bound) created during photoexcitation and it corresponds to the difference between the quasiparticle band gap and the absolute energy of the exciton transition (I). For our monolayer SnO_2 example, using the quasiparticle direct (indirect) band gap of 6.92 eV (6.51) eV, we obtain a direct (indirect) exciton binding energy of 1.56 (1.15 eV) for the lowest energy exciton. The rather high E_b is a signature of a bound exciton, which implies stability against thermal dissociation of the excitonic states that will dominate the room-temperature optical response and nonequilibrium dynamics of monolayer SnO_2. Hence, this property makes this material a candidate for exploring room-temperature optical device applications. Such a tightly bound exciton also highlights strong screening effects, which is a hallmark of atomically thin materials [44]. We, however, note that the calculated binding energy is large when compared to other 2D materials [40,41,43–47]. Another structure could be seen at ~6.05 and 6.55 eV (II), a dip is observed around 6.87 eV, and then a shoulder around 7.50 eV (III) before a sharp structure at 8.07 eV (IV). We also observed a structure around ~8.67 eV followed by two prominent peaks at 9.10 and 9.40 eV (V), respectively. Another noticeable feature is a shoulder around 10.40 eV (VI) before the spectra systematically decay to zero at higher energies (not shown). The calculated dispersive part of the dynamical dielectric function $\varepsilon_1(\omega)$ is shown in Fig. 4(b). The main features are a peak at 5.25 eV followed by a steep decrease leading to a negative $\varepsilon_1(\omega)$ with a minimum at 5.42 eV before sharply increasing toward zero. This excitation is from the direct optical transition [structure I in Fig. 4(a)]. Just as in $\varepsilon_2(\omega)$, $\varepsilon_1(\omega)$ shows strong photon-energy dependence with the features in agreement with the ones already described in Fig. 4(a).

We analyze the related transitions corresponding to the observed structures associated with the VBM, CBM, and some conduction band states along the Γ-K point of the reciprocal space. Such transitions include the optically allowed bright excitons (dominated by momentum-allowed electron-hole pair excitations) and the dark excitons (dominated by momentum-forbidden electron-hole pair excitations) as well

as localized excitons (dominated by trapped electron-hole pair excitations). The states associated with the VBM are mainly of p antibonding with some d states. The direct excitation [structure I in Fig. 4(a)] is dominated by a transition between O-p at the VBM with Sn-s and O-p states in the lowest SnO_2 conduction band. Structures II–V are dominated by the interband transition of O-p, Sn-p, and Sn-d to Sn-5s and O-p while the feature at VI and beyond is predominantly due to a complex transition between O-p with some O-s character and Sn-p states. Specifically, the small structure around 6.05 eV is a nearly dark exciton that could be associated with the second excited excitonic states. This structure hybridized slightly with the next exciton states at ∼6.55 eV.

To further explore the excitonic states and the origin of the rather large exciton binding energy in monolayer SnO_2, we employ a simple exciton model. Intuitively, because of quantum confinement, low-dimensional materials exhibit poor dielectric screening. Moreover, when the quasiparticle band gap is large, nonlocal screening effect is even weaker due to the narrow spatial overlap of the density of occupied and unoccupied states. Because of this narrow spatial extension of the wave function of states in the proximity of the Fermi level coupled with the long-ranged electron-hole interactions, the exciton radius will be reduced leading to higher binding energy. This observation is supported by recent first-principles calculations that show linear scaling of E_b and the quasiparticle band gap [13,48]. To test this premise, we note that the macroscopic dielectric function is related to the polarizability as $\alpha(\vec{q}) = c\,\frac{\varepsilon(\vec{q})-1}{4\pi}$ [49], where $c \sim 20$ Å. Evaluating this relation on a set of small $\vec{q}$ points, we obtain $\alpha \sim 1.31$ Å. When we adopt the screened hydrogen model [48,50], $E_b = \frac{8\mu e^4}{\hbar^2[1+\sqrt{1+32\pi\mu\,(e/\sqrt{3}\hbar)^2}]^2} \approx \frac{3E_g}{2N_g}$ [50]. Herein, $N_g = 9$ (composed of O-p, Sn-s, and Sn-d states) is the number of bands participating in the band-gap formation along the Γ-K direction of the high-symmetry points. Using these values, we obtain $E_b \sim 1.09$ eV, which is in reasonable agreement (differing by only ∼5.65%) with the binding energy obtained from our first-principles Bethe-Salpeter theory.

In summary, we report the optical properties of monolayer SnO_2 obtained from first-principles many-body calculations. To ensure the accurate description of the electron-electron and electron-hole interactions, which are important for the electronic and optical properties, we used several levels of theory. By calculating the quasiparticle states within the self-consistent quasiparticle GW approach, we show that monolayer SnO_2 is an indirect gap semiconductor with a band gap of 6.51 eV and a minimum direct band gap of 6.92 eV. In order to obtain the optical spectra, we solved the Bethe-Salpeter equation. A detailed analysis of the first few exciton features in the proximity of the optical band gap suggests that these structures are derived from the interband transitions across a direct optical gap of ∼5.36 eV in the presence of strong electron-hole interactions. We deduced the binding energy of these tightly bound excitons to be in excess of 1.0 eV predicted both from our first-principles Bethe-Salpeter theory and the screened hydrogen model.

The research was sponsored by the Army Research Laboratory (ARL) and was accomplished under the Cooperative Agreement No. W911NF-11-2-0030 as an ARL Research [George F. Adams] Fellow. Supercomputer support is provided by the DOD High-Performance Computing Modernization Program at the Army Engineer Research and Development Center, Vicksburg, MS.

[1] O. Madelung, U. Rössler, and M. E. Schulz, *Numerical Data and Functional Relationships in Science and Technology, Landolt-Börnstein, New Series, Group III*, Vols. 17a and 22a (Springer, Berlin, 2006).

[2] W. Göpel and K. D. Schierbaum, Sens. Actuators, B **26**, 1 (1995); R. Lalauze and C. Pijolat, *ibid.* **5**, 55 (1984); S. Das and V. Jayaraman, Prog. Mater. Sci. **66**, 112 (2014); P. G. Harrison and M. J. Willett, Nature (London) **332**, 337 (1988).

[3] H. J. Snaith and C. Ducati, Nano Lett. **10**, 1259 (2010).

[4] K. Ellmer, Nat. Photon. **6**, 809 (2012); R. G. Gordon, MRS Bull. **25**, 52 (2000); S. C. Dixon, D. O. Scanlon, C. J. Carmalt, and I. P. Parkin, J. Mater. Chem. C **4**, 6946 (2016); J. S. Chen and X. W. D. Lou, Small **9**, 1877 (2013); C. J. Martinez, B. Hockey, C. B. Montgomery, and S. Semancik, Langmuir **21**, 7937 (2005); A. K. Singh, A. Janotti, M. Scheffler, and C. G. Van de Walle, Phys. Rev. Lett. **101**, 055502 (2008).

[5] M. Stefik, M. Cornuz, N. Mathews, T. Hisatomi, S. Mhaisalkar, and M. Grätzel, Nano Lett. **12**, 5431 (2012).

[6] L. Jiang, G. Sun, Z. Zhou, S. Sun, Q. Wang, S. Yan, H. Li, J. Tian, J. Guo, B. Zhou, and Q. Xin, J. Phys. Chem. B **109**, 8774 (2005).

[7] K. Gotlib-Vainstein, I. Gouzman, O. Girshevitz, A. Bolker, N. Atar, E. Grossman, and C. N. Sukenik, ACS Appl. Mater. Interfaces **7**, 3539 (2015).

[8] Z. W. Pan, Z. R. Dai, and Z. L. Wang, Science **291**, 1947 (2001); A. Kolmakov, D. O. Klenov, Y. Lilach, S. Stemmer, and M. Moskovits, Nano Lett. **5**, 667 (2005).

[9] Y. Zhang, A. Kolmakov, S. Chretien, H. Metiu, and M. Moskovits, Nano Lett. **4**, 403 (2004); D. Sirbuly, A. Tao, M. Law, R. Fan, and P. Yang, Adv. Mater. **19**, 61 (2007).

[10] P. Hohenberg and W. Kohn, Phys. Rev. **136**, B864 (1964); W. Kohn and L. J. Sham, *ibid.* **140**, A1133 (1965).

[11] J. P. Perdew, K. Burke, and M. Ernzerhof, Phys. Rev. Lett. **77**, 3865 (1996).

[12] D. Y. Qiu, F. H. da Jornada, and S. G. Louie, Phys. Rev. Lett. **111**, 216805 (2013); Phys. Rev. B **93**, 235435 (2016); F. A. Rasmussen, P. S. Schmidt, K. T. Winther, and K. S. Thygesen, *ibid.* **94**, 155406 (2016).

[13] J.-H. Choi, P. Cui, H. Lan, and Z. Zhang, Phys. Rev. Lett. **115**, 066403 (2015).

[14] F. Hüser, T. Olsen, and K. S. Thygesen, Phys. Rev. B **87**, 235132 (2013); **88**, 245309 (2013).

[15] M. Shishkin, M. Marsman, and G. Kresse, Phys. Rev. Lett. **99**, 246403 (2007); M. Shishkin and G. Kresse, Phys. Rev. B **75**, 235102 (2007); **74**, 035101 (2006); M. van Schilfgaarde, T. Kotani, and S. Faleev, Phys. Rev. Lett. **96**, 226402 (2006).

[16] F. Gross, *Relativistic Quantum Mechanics and Field Theory* (Wiley, New York, 1999).

[17] E. Gross, E. Runge, and O. Heinonen, *Many-Particle Theory* (A. Hilger, Bristol, UK, 1991).

[18] J. W. Negele and H. Orland, *Quantum Many-Particle Systems* (Westview Press, Boulder, CO, 1998).

[19] A. Fetter and J. Walecka, *Quantum Theory of Many-Particle Systems* (Dover, New York, 1971).

[20] S. V. Faleev, M. van Schilfgaarde, and T. Kotani, Phys. Rev. Lett. **93**, 126406 (2004).

[21] L. Hedin, Phys. Rev. **139**, A796 (1965).

[22] G. Kresse and J. Furthmüller, Comput. Mater. Sci. **6**, 15 (1996).

[23] See Supplemental Material at http://link.aps.org/supplemental/10.1103/PhysRevB.99.075421 for the input files of the calculations.

[24] J. H. Jung, C.-H. Park, and J. Ihm, Nano Lett. **18**, 2759 (2018).

[25] W. Wang, S. Dai, X. Li, J. Yang, D. J. Srolovitz, and Q. Zheng, Nat. Commun. **6**, 7853 (2015).

[26] S. Lebègue, J. Harl, T. Gould, J. G. Ángyán, G. Kresse, and J. F. Dobson, Phys. Rev. Lett. **105**, 196401 (2010); A. K. Singh and R. G. Hennig, Appl. Phys. Lett. **105**, 042103 (2014); T. Björkman, A. Gulans, A. V. Krasheninnikov, and R. M. Nieminen, Phys. Rev. Lett. **108**, 235502 (2012).

[27] T. A. Manz, RSC Adv. **7**, 45552 (2017).

[28] T. A. Manz and N. G. Limas, RSC Adv. **6**, 47771 (2016); A. V. Krukau, O. A. Vydrov, A. F. Izmaylov, and G. E. Scuseria, J. Chem. Phys. **125**, 224106 (2006); J. Heyd, G. E. Scuseria, and M. Ernzerhof, *ibid.* **124**, 219906 (2006); **118**, 8207 (2003).

[29] W.-Z. Xiao, G. Xiao, and L.-L. Wang, J. Chem. Phys. **145**, 174702 (2016).

[30] F. A. Rasmussen and K. S. Thygesen, J. Phys. Chem. C **119**, 13169 (2015).

[31] J. B. Varley, A. Janotti, and C. G. Van de Walle, Phys. Rev. B **81**, 245216 (2010).

[32] J. L. Lyons, A. Janotti, and C. G. Van de Walle, Appl. Phys. Lett. **95**, 252105 (2009); M. Behtash, P. H. Joo, S. Nazir, and K. Yang, J. Appl. Phys. **117**, 175101 (2015).

[33] G. Onida, L. Reining, and A. Rubio, Rev. Mod. Phys. **74**, 601 (2002).

[34] M. van Schilfgaarde, T. Kotani, and S. V. Faleev, Phys. Rev. B **74**, 245125 (2006).

[35] P. Barbarat, S. F. Matar, and G. Le Blevennec, J. Mater. Chem. **7**, 2547 (1997).

[36] P. Blaha, K. Schwarz, G. Madsen, D. Kvasnicka, J. Luitz, F. Laskowski, F. Tran, and L. D. Marks, *WIEN2K, An Augmented Plane Wave+Local Orbitals Program for Calculating Crystal Structure* (K. Schwarz Technical University, Wien, Austia, 2018).

[37] K. G. Godinho, A. Walsh, and G. W. Watson, J. Phys. Chem. C **113**, 439 (2009).

[38] A. Svane and E. Antoncik, J. Phys. Chem. Solids **48**, 171 (1987).

[39] J. Liu, X. Qian, and L. Fu, Nano Lett. **15**, 2657 (2015).

[40] A. Hanbicki, M. Currie, G. Kioseoglou, A. Friedman, and B. Jonker, Solid State Commun. **203**, 16 (2015).

[41] T. C. Doan, J. Li, J. Y. Lin, and H. X. Jiang, Appl. Phys. Lett. **109**, 122101 (2016).

[42] C. E. Ekuma and D. Gunlycke, Phys. Rev. B **97**, 201414 (2018).

[43] M. M. Ugeda, A. J. Bradley, S.-F. Shi, F. H. da Jornada, Y. Zhang, D. Y. Qiu, W. Ruan, S.-K. Mo, Z. Hussain, Z.-X. Shen, F. Wang, S. G. Louie, and M. F. Crommie, Nat. Mater. **13**, 1091 (2014).

[44] B. Arnaud, S. Lebègue, P. Rabiller, and M. Alouani, Phys. Rev. Lett. **96**, 026402 (2006).

[45] B. Radisavljevic and A. Kis, Nat. Mater. **12**, 815 (2013).

[46] A. F. Rigosi, H. M. Hill, K. T. Rim, G. W. Flynn, and T. F. Heinz, Phys. Rev. B **94**, 075440 (2016); H. M. Hill, A. F. Rigosi, C. Roquelet, A. Chernikov, T. C. Berkelbach, D. R. Reichman, M. S. Hybertsen, L. E. Brus, and T. F. Heinz, Nano Lett. **15**, 2992 (2015); C. Zhang, A. Johnson, C.-L. Hsu, L.-J. Li, and C.-K. Shih, *ibid.* **14**, 2443 (2014); A. R. Klots, A. K. M. Newaz, B. Wang, D. Prasai, H. Krzyzanowska, J. Lin, D. Caudel, N. J. Ghimire, J. Yan, B. L. Ivanov, K. A. Velizhanin, A. Burger, D. G. Mandrus, N. H. Tolk, S. T. Pantelides, and K. I. Bolotin, Sci. Rep. **4**, 6608 (2014); Y. Yu, Y. Yu, Y. Cai, W. Li, A. Gurarslan, H. Peelaers, D. E. Aspnes, C. G. Van de Walle, N. V. Nguyen, Y.-W. Zhang, and L. Cao, *ibid.* **5**, 16996 (2015).

[47] H. L. Zhuang and R. G. Hennig, Phys. Rev. B **88**, 115314 (2013); M. Sajjad, N. Singh, and U. Schwingenschlögl, Appl. Phys. Lett. **112**, 043101 (2018).

[48] T. Olsen, S. Latini, F. Rasmussen, and K. S. Thygesen, Phys. Rev. Lett. **116**, 056401 (2016).

[49] T. C. Berkelbach, M. S. Hybertsen, and D. R. Reichman, Phys. Rev. B **88**, 045318 (2013); L. Wirtz, A. Marini, and A. Rubio, Phys. Rev. Lett. **96**, 126104 (2006).

[50] Z. Jiang, Z. Liu, Y. Li, and W. Duan, Phys. Rev. Lett. **118**, 266401 (2017).